J|A|C|S ARTICLES

Published on Web 03/06/2009

Binding Mechanism of an SH3 Domain Studied by NMR and ITC

Jean-Philippe Demers and Anthony Mittermaier*

Department of Chemistry, McGill University, 801 Sherbrooke Street West, Montreal, Quebec, Canada, H3A 2K6

Received October 21, 2008; E-mail: anthony.mittermaier@mcgill.ca

Abstract: Complexes between Src-homology 3 domains and proline-rich target peptides can have lifetimes on the order of milliseconds, making them too short-lived for kinetic characterization by conventional methods. Nuclear magnetic resonance (NMR) dynamics experiments are ideally suited to study such rapid binding equilibria, and additionally provide information on partly bound intermediate states. We used NMR together with isothermal titration calorimetry (ITC) to characterize the interaction of the SH3 domain from the Fyn tyrosine kinase with a 12-residue peptide at temperatures between 10 and 50 °C. NMR data at all temperatures are consistent with an effectively two-state binding reaction, such that any intermediates are either very weakly populated or exchange extremely rapidly with the free or bound forms. Dissociation rate constants, determined by CPMG and ZZ-exchange NMR experiments, range from $k_{off}(10\ °C) = 4.5\ s^{-1}$ to $k_{off}(50\ °C) = 331\ s^{-1}$. ITC data at all temperatures follow a simple two-state interaction model. Binding is favored enthalpically, with a dissociation enthalpy, $\Delta H_D(30\ °C) = 15.4$ kcal mol^{-1}, and disfavored entropically, with a dissociation entropy, $\Delta S_D(30\ °C) = 20.0$ cal mol^{-1} K^{-1}. The free protein and peptide have significantly higher heat capacity than the bound complex, $\Delta C_p = 352$ cal mol^{-1} K^{-1}, which is consistent with the largely hydrophobic character of the binding interface. An Eyring plot of k_{off} values gives an activation enthalpy of dissociation, $\Delta H_D^{\ddagger}(30\ °C) = 19.3$ kcal mol^{-1} and exhibits slight curvature consistent with the ITC-derived value of ΔC_p. The curvature suggests that nonpolar residues of the hydrophobic interface are solvated in the transition state for dissociation. Association rate constants were calculated as $k_{on} = k_{off}/K_D$, and range from $k_{on}(10\ °C) = 1.03 \times 10^8\ M^{-1}\ s^{-1}$ to $k_{on}(50\ °C) = 2.0 \times 10^8\ M^{-1}\ s^{-1}$, with an apparent activation enthalpy, $\Delta H_A^{\ddagger} = 3.4$ kcal mol^{-1}. Both the magnitudes and temperature dependence of k_{on} values are consistent with a diffusion-limited association mechanism. The combination of NMR and ITC data sheds light on how the Fyn tyrosine kinase is activated by binding to proline-rich targets, and represents a powerful approach for characterizing transient protein/ligand interactions.

Introduction

Living systems depend on tightly regulated networks of protein/ligand interactions. In many cases, it is necessary that complexes form rapidly as well as bind tightly.[1−3] This raises a problem analogous to that of protein folding: how do binding partners rapidly select the correct conformations and relative orientations for productive interaction from the landscape of different options? Numerous theoretical, computational, and experimental studies have addressed this question.[4−9] However, there are still some aspects of the process that are not well understood. For example, it can be difficult to assess the extent to which partly bound intermediates are formed during the association process. As well, most highly studied systems bind very tightly and dissociate very slowly, with bound lifetimes on the order of hours or days. Much less is known about weaker complexes with bound lifetimes on the order of milliseconds.

Nuclear Magnetic Resonance (NMR) spectroscopy is well-suited to address these issues. It can be applied to weakly bound systems with very rapid dissociation rates, and it is sensitive to the presence of binding intermediates. In a typical, non-NMR binding experiment, the reaction is initiated by the rapid addition of ligand, and the progress of the reaction is detected in real time, using a variety of measures including fluorescence,[10−12] spectroscopic absorbance,[13] surface plasmon resonance,[14,15] or enzymatic activity.[16−18] The lifetimes of the free and bound states must be several-fold longer than the time required to completely mix the protein and ligand solutions, otherwise the reaction proceeds nearly to completion before the start of the measurement period. In contrast, there is no dead-time for NMR

(1) Foote, J.; Milstein, C. *Nature* **1991**, *352*, 530–532.
(2) Wang, Y. H.; Shen, B. J.; Sebald, W. *Proc. Natl. Acad. Sci. U.S.A.* **1997**, *94*, 1657–1662.
(3) Jucovic, M.; Hartley, R. W. *Proc. Natl. Acad. Sci. U.S.A.* **1996**, *93*, 2343–2347.
(4) Gabdoulline, R. R.; Wade, R. C *Curr. Opin. Struct. Biol.* **2002**, *12*, 204–213.
(5) Janin, J. *Proteins Struct. Funct. Genet.* **1997**, *28*, 153–161.
(6) Berg, O. G.; Vonhippel, P. H. *Ann. Rev. Biophys. Chem.* **1985**, *14*, 131–160.
(7) Zhou, H. X. *Phys. Biol.* **2005**, *2*, R1–R25.
(8) Schreiber, G.; Fersht, A. R *Nat. Struct. Biol.* **1996**, *3*, 427–431.
(9) Zhou, H. X.; Wlodek, S. T.; McCammon, J. A. *Proc. Natl. Acad. Sci. U.S.A.* **1998**, *95*, 9280–9283.
(10) Schreiber, G.; Fersht, A. R. *Biochemistry* **1993**, *32*, 5145–5150.
(11) Sydor, J. R.; Engelhard, M.; Wittinghofer, A.; Goody, R. S.; Herrmann, C. *Biochemistry* **1998**, *37*, 14292–14299.
(12) Wallis, R.; Moore, G. R.; James, R.; Kleanthous, C. *Biochemistry* **1995**, *34*, 13743–13750.

measurements of binding rates, since the experiment is conducted under equilibrium conditions. Kinetic information is derived from a quantitative analysis of the magnetization transfer and spectral broadening produced by the exchange between bound and free states in a partially ligand-saturated sample. NMR dynamics analyses can be applied to systems with dissociation rates of greater than 10^4 s^{-1},[19] which is above the above the upper limit of nonequilibrium mixing experiments. NMR is also able to discriminate between two-state and multistate binding mechanisms, since each nucleus in the protein and ligand whose chemical shift changes upon complex formation represents an independent probe of the binding reaction. The existence of binding intermediates may be inferred when data for multiple nuclei are incompatible with a global two-state mechanism.[20] In comparison, a typical nonequilibrium mixing experiment monitors the binding reaction with a single observable and a consistency test of this sort is not possible.

NMR line-shape analysis has been used to determine the rates of reversible chemical reactions for many years,[21] and more recent investigations have produced quantitative models of protein interactions from NMR relaxation data.[20,22−30] In this study, we used a combination of multidimensional NMR dynamics experiments and isothermal titration calorimetry (ITC) to characterize the interaction between the SH3 domain from the Fyn tyrosine kinase and a 12-residue peptide. SH3 domains are small (∼60 aa), eukaryotic, protein interaction modules that participate in a variety of protein signaling networks and bind to proline-rich sequences in their targets with affinities on the order of μM.[31−35] SH3 domains interact promiscuously with different peptide sequences, which may be separated into two classes, based on the relative orientation of the peptide chain within the binding site. The peptide used in this study (VSLARRPLPPLP)[36] follows the type I consensus sequence, +xΦPxΦP, where (+) is a positively charged residue, (P) is proline, (Φ) is a hydrophobic residue and (x) is any residue.[37] The binding interface is predominantly nonpolar, but includes an acidic patch adjacent to the peptide arginine side chains. The relatively low affinity of this system suggested that binding kinetics would be on the millisecond time scale, and therefore ideal for study by NMR. In fact, we obtained dissociation rate constants of this order.

In the case of a two-state binding reaction, the kinetics of exchange follow,

$$\mathrm{P} \underset{k_{\mathrm{off}}}{\overset{k_{\mathrm{on}}[\mathrm{X}]}{\rightleftharpoons}} \mathrm{PX} \qquad (1)$$

where P and PX correspond to the free and bound protein states, respectively, k_{off} is the first-order dissociation rate constant, k_{on} is the second-order association rate constant, and [X] is the concentration of uncomplexed peptide in solution. We prepared an NMR sample in which the protein was partially saturated with peptide and used a combination of ZZ-exchange[38−40] and Carr−Purcell−Meiboom−Gill (CPMG)[19] relaxation dispersion NMR experiments to precisely measure k_{off} and k_{on}[X]. The equilibrium dissociation constant, K_{D}, of this interaction is much lower than the concentrations of protein and peptide required for the NMR sample, i.e., $[\mathrm{P}]_{\mathrm{total}} > [\mathrm{X}]_{\mathrm{total}} \gg K_{\mathrm{D}}$. As a result, the concentration of free peptide, [X], is on the order of nanomolar, and the concentration of the bound state is governed only by the total concentration of peptide, $[\mathrm{PX}] \approx [\mathrm{X}]_{\mathrm{total}}$. This has two important consequences. First, because [PX] is nearly independent of K_{D} at these concentrations, the affinity of the interaction cannot be determined by NMR titration analysis. Second, because [X] is vanishingly small, the association rate constants cannot be extracted directly from experimentally determined k_{on}[X] values. In order to determine k_{on} values, equilibrium dissociation constants, K_{D}, were measured by ITC, and used together with NMR-derived k_{off} values to calculate association rate constants according to the following:

$$k_{\mathrm{on}} = \frac{k_{\mathrm{off}}}{K_{\mathrm{D}}} \qquad (2)$$

ITC requires much lower protein and peptide concentrations than does NMR, therefore K_{D} values could be accurately measured by this technique.

The experimental approach used in this study can be applied to wide variety of other transiently interacting systems. NMR dynamics techniques are applicable to proteins with molecular weights in excess of 300 kDa[41] and with dissociation rate constants, k_{off}, between approximately 1 s^{-1} and 10^4 s^{-1}.[19,40] ITC can be used to determine equilibrium dissociation constants ranging from below 1 nM [42,43] to above 10 mM.[44] For systems

(13) Northrup, S. H.; Thomasson, K. A.; Miller, C. M.; Barker, P. D.; Eltis, L. D.; Guillemette, J. G.; Inglis, S. C.; Mauk, A. G. *Biochemistry* **1993**, *32*, 6613–6623.
(14) England, P.; Bregegere, F.; Bedouelle, H. *Biochemistry* **1997**, *36*, 164–172.
(15) Altschuh, D.; Dubs, M. C.; Weiss, E.; Zederlutz, G.; Vanregenmortel, M. H. V. *Biochemistry* **1992**, *31*, 6298–6304.
(16) Stone, S. R.; Dennis, S.; Hofsteenge, J. *Biochemistry* **1989**, *28*, 6857–6863.
(17) Taylor, M. G.; Rajpal, A.; Kirsch, J. F *Protein Sci.* **1998**, *7*, 1857–1867.
(18) Radic, Z.; Kirchhoff, P. D.; Quinn, D. M.; McCammon, J. A.; Taylor, P *J. Biol. Chem.* **1997**, *272*, 23265–23277.
(19) Palmer, A. G.; Kroenke, C. D.; Loria, J. P. *Methods Enzymol.* **2001**, *339*, 204–238.
(20) Sugase, K.; Dyson, H. J.; Wright, P. E. *Nature* **2007**, *447*, 1021–U11.
(21) McConnell, H. M. *J. Chem. Phys.* **1958**, *28*, 430–431.
(22) Feher, V. A.; Baldwin, E. P.; Dahlquist, F. W *Nat. Struct. Biol.* **1996**, *3*, 516–521.
(23) Malmendal, A; Evenas, J; Forsen, S; Akke, M *J. Mol. Biol.* **1999**, *293*, 883–899.
(24) Sahu, D.; Clore, G. M.; Iwahara, J *J. Am. Chem. Soc.* **2007**, *129*, 13232–13237.
(25) Iwahara, J.; Zweckstetter, M.; Clore, G. M. *Proc. Natl. Acad. Sci. U.S.A.* **2006**, *103*, 15062–15067.
(26) Tang, C.; Iwahara, J.; Clore, G. M. *Nature* **2006**, *444*, 383–386.
(27) Vallurupalli, P.; Hansen, D. F.; Stollar, E.; Meirovitch, E.; Kay, L. E. *Proc. Natl. Acad. Sci. U.S.A.* **2007**, *104*, 18473–18477.
(28) Mittag, T; Schaffhausen, B; Gunther, U. L *J. Am. Chem. Soc.* **2004**, *126*, 9017–9023.
(29) Mittag, T.; Schaffhausen, B.; Gunther, U. L. *Biochemistry* **2003**, *42*, 11128–11136.
(30) Tolkatchev, D.; Xu, P.; Ni, F *J. Am. Chem. Soc.* **2003**, *125*, 12432–12442.
(31) Koch, C. A.; Anderson, D.; Moran, M. F.; Ellis, C.; Pawson, T. *Science* **1991**, *252*, 668–674.
(32) Kuriyan, J.; Cowburn, D. *Curr. Opin. Struct. Biol.* **1993**, *3*, 828–837.
(33) Mayer, B. J.; Hamaguchi, M.; Hanafusa, H. *Nature* **1988**, *332*, 272–275.
(34) Musacchio, A.; Wilmanns, M.; Saraste, M. *Prog. Biophys. Mol. Biol.* **1994**, *61*, 283–297.
(35) Pawson, T.; Gish, G. D. *Cell* **1992**, *71*, 359–362.
(36) Rickles, R. J.; Botfield, M. C.; Zhou, X. M.; Henry, P. A.; Brugge, J. S.; Zoller, M. J. *Proc. Natl. Acad. Sci. U.S.A.* **1995**, *92*, 10909–10913.
(37) Mayer, B. J. *J. Cell Sci.* **2001**, *114*, 1253–1263.
(38) Wider, G.; Neri, D.; Wüthrich, K. *J. Biomol. NMR* **1991**, *1*, 93–98.
(39) Montelione, G. T.; Wagner, G. *J. Am. Chem. Soc.* **1989**, *111*, 3096–3098.
(40) Farrow, N. A.; Zhang, O.; Forman-Kay, J. D.; Kay, L. E. *J. Biomol. NMR* **1994**, *4*, 727–734.

with $K_D \geq 10\ \mu M$, NMR titration analyses can also be used to determine binding affinities,[45] however ITC experiments are still preferable for $K_D \leq 100\ \mu M$, since they provide a direct measure of the binding enthalpy.[44] The most stringent requirements of this approach are that (1) the proteins under investigation are soluble at relatively high concentration ($>100\ \mu M$) and provide well-resolved NMR spectra and (2) the proteins and ligands can be obtained in relatively large amounts: 0.1 to 1 μmoles for NMR dynamics experiments and 10 to 100 nmoles for ITC measurements. Note that in the weak-binding regime with $K_D > 100\ \mu M$, relatively high concentrations of free ligand, [X], are present in the partly saturated samples used for NMR dynamics experiments, and in principle k_{on} can be determined directly from $k_{on}[X]$.

We performed NMR and ITC experiments on the Fyn SH3 domain and 12-residue peptide at temperatures ranging from 10 to 50 °C. The combined data set provided detailed information not accessible from either the NMR or ITC measurements alone. Using NMR, we tested for the existence of well-populated binding intermediates, extracted dissociation rate constants, and from their temperature dependence characterized the energy barrier to dissociation. Using ITC, we extracted the equilibrium constants, enthalpies and entropies of dissociation, and fitted their temperature dependences to obtain the difference in heat capacity between the free and bound states. With the combined NMR and ITC data set, we calculated association rate constants, and from their temperature dependence characterized the rate-determining step of association. In addition, the comparison of the NMR and ITC results provided an element of cross-validation between the two techniques: association rate constants calculated with a combination of NMR and ITC data are physically reasonable, exhibiting both the magnitude and temperature dependence typical of a diffusion-limited reaction, while curvature of the Eyring plot of NMR-derived dissociation rates matches the ITC-derived heat capacity value. The internal consistency of the combined data set highlights the potential of using NMR and calorimetry in concert to quantitate functional dynamics in proteins.

Experimental Section

Peptide Ligands. A peptide with the sequence Ac-VSLAR-RPLPPLP-NH_2 was synthesized by the Sheldon Biotechnology Centre (McGill, Montreal), and purified to >98% homogeneity by reverse-phase HPLC. A MW of 1356.85 Da was confirmed by mass spectrometry. The peptide powder was dissolved in water and dialyzed against 20 mM sodium phosphate, 1 mM EDTA, pH 6.0. The concentration of the dialyzed solution was estimated by amino acid analysis (The Hospital for Sick Children, Toronto). Samples were hydrolyzed in 6 M HCl, 1% phenol for 24 h at 110 °C, derivatized with phenylisothiocyanate to produce phenylthiocarbamyl amino acids, and quantified by reverse-phase HPLC. The errors in amino acid analyses are typically 10%, but can range from approximately 5% to 50%.[46,47]

Protein Sample Preparation. The protein samples used in this studied were produced with a pET11d-based expression plasmid (Novagen) coding for the SH3 domain (residues 81 to 148) of the chicken isoform of the Fyn tyrosine kinase fused to an N-terminal 6-histidine affinity purification tag. Proteins for ITC studies were expressed in freshly transformed *E. coli* BL21(DE3) bacteria grown at 37 °C in Luria broth (LB). Expression was induced at an OD_{600} of 0.8 by adding 200 mg L^{-1} IPTG (isopropyl β-D-1-thiogalactopyranoside). Cells were harvested by centrifugation 3 h later. Isotopically labeled proteins were expressed according to the protocol of Marley et al.[48] Bacteria were first cultured in 4 L of LB to an OD_{600} of 0.8, then transferred to 1 L of M9 minimal media, which contained $^{15}NH_4Cl$ and D-glucose as the sole sources of nitrogen and carbon. In the case of samples used for triple-resonance assignment experiments, the D-glucose was uniformly ^{13}C labeled. Expression was induced 1 h after the transfer to M9 media and cells were harvested by centrifugation after a further 3 h. Protein purification was performed with a modified protocol based on that of Maxwell and Davidson.[49] Cell pellets were resuspended in a solution containing 0.1 M NaH_2PO_4, 0.01 M Tris, 6 M Gdm-Hcl, and 0.01 M imidazole, at pH 8.0 and rocked for 1 h at room temperature to achieve lysis. The lysate was centrifuged, and the supernatant was applied to a Toyopearl AF-Chelate-650 M column (Tosoh Bioscience). The column was washed extensively with lysis buffer and the protein was eluted with a solution containing 0.2 M acetic acid and 6 M Gdm-HCl. The eluate was dialyzed against a solution containing 150 mM NaCl, 50 mM Tris, 2 mM EDTA, and 5 mM benzamidine, at pH 7.9, and purified by size-exclusion chromatography using a Superdex 75 10/300 GL column (GE HealthSciences). The elution volume of the protein corresponded to the nominal molecular weight of the desired product, 8.7 kDa. Sample purity was estimated by SDS-PAGE to be greater than 99%. Protein concentration was estimated using a theoretical 280 nm extinction coefficient.[50]

NMR Spectroscopy. All NMR experiments were performed on protein samples containing 20 mM sodium phosphate, pH 6.0, 1 mM EDTA, 10 μM DSS (dimethyl-silapentane-sulfonate) 0.02% sodium azide, and 10% D_2O. NMR spectra were recorded on Varian INOVA spectrometers operating at 800 and 500 MHz proton Larmor frequencies, (18.8 and 11.7 T), equipped with high-sensitivity cold-probes. All 2D spectra were processed with shifted sine-bell weighting functions in the t_1 (^{15}N) and t_2 (^1H) dimensions. Chemical shifts and peak intensities were fitted using the nlinLS program of the nmrPipe package.[51]

Spectral Assignment. All 66 backbone amide resonances, except those of the 6-histidine tag, were assigned using HNCACB spectra,[52] recorded at 30 °C and 18.8 T for the Fyn SH3 domain in both the peptide-free (0.34 mM Fyn) and peptide-saturated (0.34 mM Fyn, 0.5 mM peptide) states. $^1H-^{15}N$ HSQC spectra[53] of the free and peptide-saturated Fyn SH3 domain were recorded at 10, 20, 30, 35, 40, 45, and 50 °C. ^1H and ^{15}N chemical shifts varied approximately linearly with temperature such that the assignments obtained at 30 °C could be propagated to the other temperatures. Accordingly, the ^{15}N chemical shift difference, $\Delta\delta_{HSQC}$, between the free and peptide-saturated resonances of the protein could be computed for all temperatures.

ZZ-Exchange Experiments. ZZ exchange NMR experiments[40] were performed at 10 and 20 °C at a proton Larmor frequency of 800 MHz, with 64 and 833 complex points in the indirect and direct

(41) Sprangers, R.; Gribun, A.; Hwang, P. M.; Houry, W. A.; Kay, L. E. *Proc. Natl. Acad. Sci. U.S.A.* **2005**, *102*, 16678–16683.
(42) Leavitt, S.; Freire, E. *Curr. Opin. Struct. Biol.* **2001**, *11*, 560–566.
(43) Sigurskjold, B. W. *Anal. Biochem.* **2001**, *277*, 260–266.
(44) Tellinghuisen, J. *Anal. Biochem.* **2008**, *373*, 395–397.
(45) Harding, S. E.; Chowdhry, B. Z. *Protein-Ligand Interactions: Structure and Spectroscopy*; Oxford University Press: Oxford, 2001; Vol. 2.
(46) Schegg, K. M.; Denslow, N. D.; Andersen, T. T.; Bao, Y.; Cohen, S. A.; Mahrenholz, A. M.; Mann, K. In *Techniques in Protein Chemistry*; Marshak, D. R, Ed.; Academic Press: Oxford, 1997; Vol. 8, p 207−216,
(47) Smith, A. J. *Methods Enzymol.* **1997**, *289*, 419–426.
(48) Marley, J.; Lu, M.; Bracken, C. *J. Biomol. NMR* **2001**, *20*, 71–75.
(49) Maxwell, K. L.; Davidson, A. R. *Biochemistry* **1998**, *37*, 16172–16182.
(50) Pace, C. N.; Vajdos, F.; Fee, L.; Grimsley, G.; Gray, T *Protein Sci.* **1995**, *4*, 2411–2423.
(51) Delaglio, F.; Grzesiek, S.; Vuister, G. W.; Zhu, G.; Pfeifer, J.; Bax, A. *J. Biomol. NMR* **1995**, *6*, 277–293.
(52) Wittekind, M.; Mueller, L. *J. Magn. Reson. Series B* **1993**, *101*, 201–205.
(53) Kay, L. E.; Keifer, P.; Saarinen, T. *J. Am. Chem. Soc.* **1992**, *114*, 10663–10665.

dimensions, collecting 32 scans for each indirect point. Mixing times, T_{mix} (labeled T in Farrow et al.[40]) of (0, 0.0214, 0.0482, 0.0856, 0.1445, 0.1927, 0.3425, 0.5352, 0.7707, 1.0490) s and (0, 0.0214, 0.0482, 0.0856, 0.1445, 0.1927, 0.3425, 0.5352, 0.7707) s were used at 10 and 20 °C, respectively. Data were fit numerically to an equation that accounts for exchange during the magnetization transfer steps:

$$\begin{bmatrix} I_{ff} & I_{bf} \\ I_{fb} & I_{bb} \end{bmatrix} = \begin{bmatrix} 1 & y_{bf} \\ y_{fb} & y_{bb} \end{bmatrix} \bullet \exp\left(T_{mix} \begin{bmatrix} -k'_{on} - R_1^f & k_{off} \\ k'_{on} & -k_{off} - R_1^b \end{bmatrix} \right) \bullet \begin{bmatrix} I_0^f & 0 \\ 0 & I_0^b \end{bmatrix} \quad (3)$$

$$k'_{on} = k_{on}[X] = k_{off}\frac{p_B}{1 - p_B} \quad (4)$$

where I_0^f and I_0^b are the amplitudes of the free and bound signals immediately before the mixing delay, R_1^f and R_1^b are the ^{15}N longitudinal relaxation rates in the free and bound states, y_{bf} and y_{fb} account for exchange and y_{bb} accounts for differential relaxation during the magnetization transfer steps that follow the mixing delay. I_{ff} and I_{bb} are the experimentally observed intensities of the free and bound autopeaks, and I_{fb} and I_{bf} are the experimentally observed intensities of the cross-peaks. The matrix exponential was calculated numerically in MATLAB. The parameters I_0^f, I_0^b, y_{fb}, y_{bf}, y_{bb}, R_1^f, and R_1^b were optimized on a per-residue basis. The values of k_{off} and p_B were optimized twice, once on a per-residue basis, and again as global parameters for all residues at a given temperature. Nonlinear fits were performed by minimizing the residual sum of squares (RSS) between experimental peak intensities and those back-calculated using eq 3. The RSS for an individual residue is given by

$$RSS = \sum_{T_{mix}} \sum_{j=ff,bb,fb,bf} [I_j^{calc}(T_{mix}) - I_j^{exp}(T_{mix})]^2 \quad (5)$$

The experimental uncertainties of k_{off} and p_B were estimated using Monte Carlo (MC) simulations with 830 iterations, according to eqs 30 and 3 with global exchange parameters. Uncertainties in peak intensities, σ_I, were estimated on a per-residue basis using the RSS from fits with individually optimized k_{off} and p_B values,

$$\sigma_I^2 = \frac{RSS}{DF} \quad (6)$$

where DF is the number of degrees of freedom of the per-residue fit, 31 for data at 10 °C and 27 at 20 °C. Equation 6 corresponds to the a posteriori estimate of measurement variance,[54] assuming equal uncertainties in all peak intensities for a given residue.

CPMG Measurements. ^{15}N CPMG single-quantum relaxation dispersion experiments were performed at 20, 30, 35, 40, 45, and 50 °C using a recently published pulse sequence that utilizes proton decoupling during the CPMG period.[55] A compensation element was applied at the beginning of each scan in order to suppress artifacts due to ν_{CPMG}-dependent changes in cold probe sensitivity.[56] CW irradiation was applied to ^{15}N nuclei for a variable time period, T_{CW}, given by:

$$(T_{CW})_i = \frac{(\nu_{CPMG})_{max} - (\nu_{CPMG})_i}{(\nu_{CPMG})_{max}} T_{relax} \quad (7)$$

where $(\nu_{CPMG})_{max}$ is the largest value of ν_{CPMG} employed in a dispersion series, typically 1000 Hz, and T_{relax} is the CPMG relaxation delay. We found that a compensation power level 8 dB below that of the CPMG pulse train provided excellent artifact suppression at both fields and all temperatures. Data obtained without this compensation element show a characteristic upward slope of roughly 1×10^{-3} s^{-1} Hz^{-1}. Flat R_2 baselines are obtained when the compensation element is included, as seen in Figure 2. Data were collected at 500 (800) MHz proton Larmor frequencies with 64 (80) and 512 (833) complex points in the indirect and direct dimensions, respectively, averaging 16 scans for each complex indirect point, with a constant relaxation delay, T_{relax}, of 40 ms. Between 12 and 24 unique values of ν_{CPMG} covering a range of 25 to 1000 Hz were used at each temperature and static magnetic field strength, where $\nu_{CPMG} = 1/(2\tau_{CP})$, and τ_{CP} is the delay between successive refocusing pulses in the CPMG pulse train. The transverse relaxation rate, R_2, was calculated for each ν_{CPMG} value according to the following:

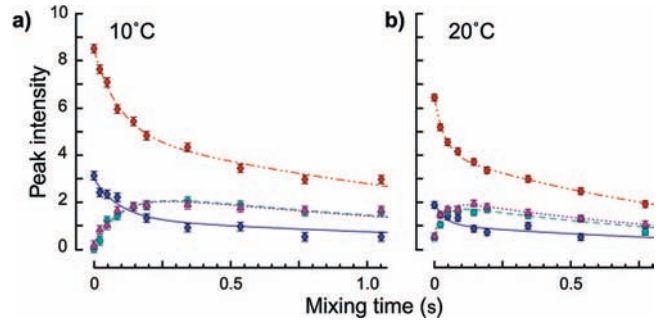

Figure 1. ZZ-exchange peak intensity profiles obtained for Gly34 of the Fyn SH3 domain in a partially ligand-saturated sample at 10 °C **(a)** and 20 °C **(b)**. Red (upper) and blue (lower) diamonds correspond to bound and free auto peak intensities. Blue circles and purple triangles correspond to association and dissociation cross peak intensities. Fitted curves were calculated using Equation (3) and globally optimized dissociation rate constants and bound state populations.

$$R_2(\nu_{CPMG}) = -\frac{1}{T_{relax}} \ln\left\{ \frac{I(\nu_{CPMG})}{I_0} \right\} \quad (8)$$

where $I(\nu_{CPMG})$ is the peak intensity obtained with a given CPMG pulse spacing and I_0 is the intensity of the peak when the relaxation delay is omitted, $T_{relax} = 0$. The uncertainty in peak intensity, σ_I, was assumed to be constant across a single dispersion profile, i.e., the same at all ν_{CPMG} values for a single residue, temperature, and static magnetic field strength. Values of σ_I were calculated for each dispersion profile using replicate spectra collected at several different ν_{CPMG} values, according to the definition of the pooled standard deviation.[57] If replicate experiments were performed at N_{dup} different ν_{CPMG} values, such that n_j replicates were obtained at $(\nu_{CPMG})_j$ and the intensities of a given peak in these n_j spectra have a standard deviation s_j, then the pooled standard deviation in peak intensity, σ_I, was calculated as follows:

$$\sigma_I^2 = \frac{\sum_{j=1}^{N_{dup}} s_j^2 (n_j - 1)}{\sum_{j=1}^{N_{dup}} (n_j - 1)} \quad (9)$$

The corresponding errors in transverse relaxation rates, σ_{R2}, across the profile are thus,

$$\sigma_{R2}(\nu_{CPMG}) = \frac{\sigma_I I_0}{T_{relax} I(\nu_{CPMG})} \quad (10)$$

(54) Tellinghuisen, J. *J. Phys. Chem.* **2000**, *104*, 2834–2844.
(55) Hansen, A. F.; Vallurupalli, P.; Kay, L. E. *J. Phys. Chem. B* **2008**, *112*, 5898–5904.
(56) Muhandiram, R.; Kay, L. E., personal communication.
(57) McNaught, A. D.; Wilkinson, A. *IUPAC Compendium of Chemical Terminology*, 2nd ed.; Royal Society of Chemistry: Cambridge, UK, 1997.

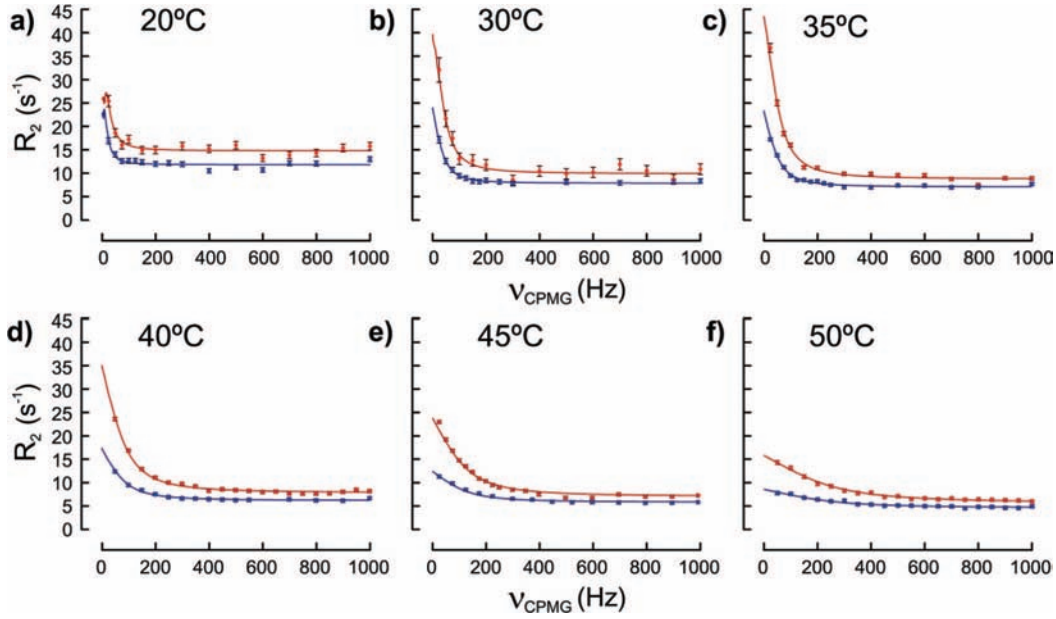

Figure 2. ^{15}N CPMG relaxation dispersion profiles obtained at 500 MHz (blue, lower) and 800 MHz (red, upper) proton Larmor frequencies for Leu7 of the Fyn SH3 domain in a partially ligand-saturated sample at 20, 30, 35, 40, 45, and 50 °C **(a)**−**(f)**. Best-fit curves were generated using Model 3, as described in the text, with fixed chemical shift differences and a temperature-independent value of the bound state population.

It has been noted that RF inhomogeneity and carrier offset effects can produce systematic deviations from ideal behavior in experimental dispersion profiles.[58,59] The extent of systematic deviations may be estimated from residues with $\Delta\omega \approx 0$, since these dispersion profiles should be flat at all temperatures and spectrometer frequencies. We defined a parameter,

$$\theta = \frac{I_{\mathrm{RMSD}}}{\sigma_{\mathrm{I}}} \tag{11}$$

where I_{rmsd} is the root-mean-squared-deviation (rmsd) of peak intensities from their mean value and σ_{I} is the estimate of experimental uncertainty derived from repeat measurements according to eq 9. This expression is equivalent to eq 2 of Ishima and Torchia.[58] When $\Delta\omega \approx 0$, peak intensities should be independent of ν_{CPMG} and the rmsd of peak intensities should match their experimental uncertainty, such that $\theta \approx 1$. If significant systematic errors are present, then σ_{I} will underestimate the variation in peak intensities and $\theta \gg 1$. We calculated θ for 231 dispersion profiles at all temperatures for residues where the free and ligand-saturated HSQC spectra indicate that $\Delta\omega < 0.1$ ppm. The mean value of θ thus obtained is 1.8, and over 75% of θ values are less than 2. This matches the empirical θ distribution for a CPMG data set that was reported to be largely free of systematic errors.[58] Furthermore, the experimental values of θ do not depend on peak position. This implies that systematic offset-dependent errors do not make a large contribution to our CPMG data sets, and that σ_{I} is a suitable estimate of experimental uncertainty.

CPMG data were fit using software generously provided by Dr. Korzhnev and Dr. Kay, which generates dispersion profiles numerically according to the following:[60]

$$R_2^{\mathrm{calc}} = -\frac{1}{T_{\mathrm{relax}}} \ln\left\{\frac{M_{\mathrm{B}}(2n_{\mathrm{CP}}\tau_{\mathrm{CP}})}{M_{\mathrm{B}}(0)}\right\} \tag{12}$$

where $2n_{\mathrm{CP}}$ refocusing pulses separated by delays of τ_{CP} are applied during the relaxation period, $T_{\mathrm{relax}} = 2n_{\mathrm{CP}}\tau_{\mathrm{CP}}$. M_{F} and M_{B} are the signals arising from the bound and free states, and are calculated following the modified Bloch−McConnell equations,

$$\begin{bmatrix} M_{\mathrm{F}}(2n_{\mathrm{CP}}\tau_{\mathrm{CP}}) \\ M_{\mathrm{B}}(2n_{\mathrm{CP}}\tau_{\mathrm{CP}}) \end{bmatrix} = \left(\exp\left(A\frac{1}{2}\tau_{\mathrm{CP}}\right)\exp(\tilde{A}\tau_{\mathrm{CP}})\exp\left(A\frac{1}{2}\tau_{\mathrm{CP}}\right)\right)^{n_{\mathrm{CP}}}\begin{bmatrix} M_{\mathrm{F}}(0) \\ M_{\mathrm{B}}(0) \end{bmatrix} \tag{13}$$

where,

$$A = \begin{bmatrix} -k'_{\mathrm{on}} - R_{2,\mathrm{F}}^{\infty} + i\Delta\omega & k_{\mathrm{off}} \\ k'_{\mathrm{on}} & -k_{\mathrm{off}} - R_{2,\mathrm{B}}^{\infty} \end{bmatrix} \tag{14}$$

$$\tilde{A} = \begin{bmatrix} -k'_{\mathrm{on}} - R_{2,\mathrm{F}}^{\infty} - i\Delta\omega & k_{\mathrm{off}} \\ k'_{\mathrm{on}} & -k_{\mathrm{off}} - R_{2,\mathrm{B}}^{\infty} \end{bmatrix} \tag{15}$$

k_{off} is the dissociation rate constant, k'_{on} is defined in eq 4, $\Delta\omega$ is the difference in precession frequency between the free and bound states, expressed in radians s^{-1}, and $R_{2,\mathrm{F}}^{\infty}$ and $R_{2,\mathrm{B}}^{\infty}$ are the transverse relaxation rates in the free and bound states in the absence of conformational exchange. We assumed that both free and bound forms of the protein experience similar rotational diffusion and internal motions and therefore have similar transverse relaxation rates in the absence of exchange. The parameters $R_{2,\mathrm{F}}^{\infty}$ and $R_{2,\mathrm{B}}^{\infty}$ in eqs 14 and 15 were therefore replaced with a single value, R_2^{∞}. The parameters k_{off}, p_{B}, $\Delta\omega$, and R_2^{∞} were fit by minimizing the chi-squared function

$$\chi^2 = \sum_{\nu_{\mathrm{CPMG}}} \frac{(R_2^{\mathrm{exp}}(\nu_{\mathrm{CPMG}}) - R_2^{\mathrm{calc}}(\nu_{\mathrm{CPMG}}))^2}{\sigma_{R2}(\nu_{\mathrm{CPMG}})^2} \tag{16}$$

according to three different local and collective dynamical models that are described later in the text. Briefly, in Model 1, k_{off}, p_{B}, and $\Delta\omega$ were fit on an individual residue basis. In Model 2, k_{off} and p_{B} were fit globally, and $\Delta\omega$ was fit locally. In Model 3, a single value of p_{B} was optimized for all temperatures, k_{off} was fit globally, and $\Delta\omega$ values were taken from HSQC spectra of the free and peptide-saturated states. Errors in the extracted parameters were estimated

(58) Ishima, R.; Torchia, D. *J. Biomol. NMR* **2005**, *32*, 41–54.
(59) Long, D.; Liu, M.; Yang, D. *J. Am. Chem. Soc.* **2008**, *130*, 2432–2433.
(60) Korzhnev, D. M.; Salvatella, X.; Vendruscolo, M.; Di Nardo, A. A.; Davidson, A. R.; Dobson, C. M.; Kay, L. E. *Nature* **2004**, *430*, 586–590.

from the covariance matrix obtained by inverting the Hessian matrix. Covariance matrix uncertainties determined by this software have been shown to closely match those obtained by Monte Carlo analyses,[61] but are far less expensive to compute, therefore they were used in the following analyses. In Models 1 and 2, under conditions of fast exchange, values of k_{ex} and Φ_{ex} were calculated from the extracted values of k_{off}, p_B, and $\Delta\omega$ according to eqs 34 and 35. A residue was selected for analysis at a given temperature if its data at 18.8 and 11.7 T met the following criteria: (i) the magnitude of the dispersion, $\max(R_2^{exp}) - \min(R_2^{exp})$ is greater than 1.0 s^{-1}; (ii) the value of χ^2 obtained with Model 1 is less than 4-fold larger than the number of degrees of freedom (no. of data points − no. of fitted parameters); (iii) The fit obtained with eq 13 is better than the fit provided by a horizontal line, at a 99.9% confidence level. Following these criteria, 19, 32, 25, 20, 20, and 22 residues were used in the analysis at 20, 30, 35, 40, 45, and 50 °C, respectively. In Model 3, optimization of the bound state population was accomplished by repeating fits with $\Delta\omega_{CPMG}$ set according to $\Delta\delta_{HSQC}$ values, and p_B fixed at 0.01 intervals between 0.66 and 0.86. The sum of χ^2 values over all temperatures shows a parabolic dependence on p_B with a minimum at $p_B = 0.74$.

Diffusion Measurements. Translational diffusion constants were measured with a room-temperature probe at 10, 20, and 30 °C and a proton Larmor frequency of 500 MHz, using a 1D ^{1}H linear-encode-decode (LED) pulsed-field-gradient (PFG) experiment[62] and samples containing either the protein alone or peptide alone. In this method, the peak intensities of the protein or peptide depend on the translational diffusion constant (D), the duration of the gradient used for encoding and decoding (δ), the time interval between the start of the encoding and decoding gradients (Δ), and the gradient strength (G_z), according to the following:

$$I = I_0 \exp\left\{-(\gamma_H \cdot \delta \cdot G_z)^2 \cdot \left(\Delta - \frac{\delta}{3}\right) \cdot D\right\} \quad (17)$$

where γ_H is the proton gyromagnetic ratio, and I_0 is the peak intensity in the absence of diffusion. We set $\delta = 2$ ms, $\Delta = 200$ ms, and varied G_z between 1.8 G cm^{-1} and 37.1 G cm^{-1} for the peptide and between 3.7 G cm^{-1} and 46.4 G cm^{-1} for the protein. The diffusion constant was extracted from a regression plot of ln{I} versus G_z^2. Integration of peak intensities was done in VNMR using a spline baseline correction.

Isothermal Titration Calorimetry. Titrations of peptide into a protein solution were carried out at 10, 20, 30, 35, 40, and 50 °C using a VP-ITC instrument (MicroCal LLC, Northampton, MA). Both peptide and protein solutions contained 20 mM sodium phosphate at pH 6.0 and 1 mM EDTA. At 20 to 50 °C, the concentrations of peptide and protein were ~0.2 mM and 0.02 mM, respectively. Experiments were done in triplicate at each temperature and consisted of 56 injections of 5 μL. At 10 °C, the concentrations of peptide and protein were ~0.04 mM and 0.004 mM, respectively. Experiments were done in duplicate, and consisted of 28 injections of 10 μL. Injections at all temperatures were made at a rate of 0.5 μL s^{-1} and at intervals of 300 s. The first injection peak was discarded from the isotherm, as were injection peaks without a stable baseline. The baseline was generated automatically by the MicroCal Origin package and corrected manually. Offsets were adjusted so that the isotherms approached 0 kcal mol^{-1} at saturating peptide concentrations.

Isotherms were fitted using the One Set of Sites model in the MicroCal Origin package, minimizing the weighted residual sum of squared deviations, SS_w, between experimental, q^{exp}, and calculated heats, q^{calc},

$$SS_w = \sum_i W_i (q_i^{exp} - q_i^{calc})^2 \quad (18)$$

The weights, W_i, were initially taken to be 1 for all data points. These fits yielded the effective number of binding sites per protein (N_b), equilibrium association constant (K_A), and enthalpy of dissociation (ΔH_D) together with the error matrix, $\hat{V}$, whose diagonal elements are the variances and whose off-diagonal are the covariances of the fitted parameters.[54] The error matrix was adjusted using an a posteriori expression for data of unknown precision,[54]

$$\hat{V}_{post} = \frac{SS_w}{DF}\hat{V} \quad (19)$$

where DF is the number of degrees of freedom of the fit. The entropy of dissociation, ΔS_D, was calculated as follows:

$$\Delta S_D = \frac{\Delta H_D}{T} - R \ln K_A \quad (20)$$

The uncertainty in ΔS_D was obtained from $\hat{V}_{post}$ according to the following:[63]

$$\sigma_S^2 = \begin{bmatrix} \frac{\partial \Delta S_D}{\partial \Delta H_D} & \frac{\partial \Delta S_D}{\partial K_A} \end{bmatrix} \hat{V}_{post} \begin{bmatrix} \frac{\partial \Delta S_D}{\partial \Delta H_D} \\ \frac{\partial \Delta S_D}{\partial K_A} \end{bmatrix} = \begin{bmatrix} \frac{1}{T} & \frac{-R}{K_A} \end{bmatrix} \begin{bmatrix} \sigma_H^2 & \rho\sigma_H\sigma_{KA} \\ \rho\sigma_H\sigma_{KA} & \sigma_{KA}^2 \end{bmatrix} \begin{bmatrix} \frac{1}{T} \\ \frac{-R}{K_A} \end{bmatrix} \quad (21)$$

where σ_S, σ_H, and σ_{KA} are the standard errors of the dissociation entropy, enthalpy, and equilibrium association constant, respectively, and ρ is the coefficient of correlation between uncertainties in ΔH_D and K_A. The equilibrium dissociation constant and the associated error were calculated as follows:

$$K_D = K_A^{-1}, \quad \sigma_{KD} = \frac{\sigma_{KA}}{K_A^2} \quad (22)$$

The default analysis in the MicroCal Origin package assumes that data are homoscedastic, i.e., all points in the ITC trace are treated as equally uncertain and are given equal weights, W_i, in eq 18. It has been shown that a variety of factors can lead to heteroscedasticity in ITC data, and that applying equal weights during fitting can reduce the precision of the extracted parameters and lead to unreliable estimates of their uncertainties.[64] The variable uncertainty of ITC data points has subsequently been modeled using generalized least-squares analyses of experimental results.[65] We used several of these uncertainty models (A, C, and E in *Tellinghuisen*[65]) to estimate individual errors for each ITC data point, $\sigma_{q,i}$, and we repeated the nonlinear least-squares minimizations with $W_i = (\sigma_{q,i})^{-2}$. The choice of weighting scheme had essentially no effect on the results of the fitting. The values of the extracted parameters from variably weighted fits deviated from those of equally weighted fits by less than 0.2%, while the estimated uncertainties deviated by less than 0.5%.

The values of ΔH_D, ΔS_D, and K_D used in the subsequent analysis were calculated as the error-weighted mean values of replicate measurements, and the experimental uncertainties were computed accordingly. For a set of N measurements, X_1 to X_N, with standard errors, $\sigma_{X,1}$ to $\sigma_{X,N}$, the error-weighted mean is given by the following:

(61) Neudecker, P.; Korzhnev, D. M.; Kay, L. E. *J. Biomol. NMR* **2006**, *34*, 129–135.
(62) Altieri, A. S.; Hinton, D. P.; Byrd, R. A *J. Am. Chem. Soc.* **1995**, *117*, 7566–7567.
(63) Tellinghuisen, J. *J. Phys. Chem. A* **2001**, *105*, 3917–3921.
(64) Tellinghuisen, J. *Anal. Biochem.* **2003**, *321*, 79–88.
(65) Tellinghuisen, J. *Anal. Biochem.* **2005**, *343*, 106–115.

$$\bar{X} = \frac{\sum_{j=1}^{N} X_j(\sigma_{X,j})^{-2}}{\sum_{j=1}^{N} (\sigma_{X,j})^{-2}} \quad (23)$$

and the standard error of the mean is as follows:

$$\sigma_{\bar{X}} = \frac{1}{\sqrt{\sum_{j=1}^{N} (\sigma_{X,j})^{-2}}} \quad (24)$$

Values of ΔH_D, ΔS_D, and K_D obtained at 10, 20, 30, 35, 40, and 50 °C were fit simultaneously to extract the difference in heat capacity between the free and bound states, ΔC_p, as well as the enthalpy and entropy of dissociation at a reference temperature of 30 °C, ΔH_0 and ΔS_0. In a standard analysis of ITC data at a single temperature, the stoichiometric parameter, N_b, serves as a correction factor for both ligand and macromolecule concentrations, and is usually required for good agreement with experimental data.[64] When fitting the multiple-temperature ITC data set, we found it necessary to introduce an additional correction factor for the concentration of the injected peptide. The requirement for this additional correction can be understood by considering the dependence of the extracted values of N_b, ΔH_D, and K_D on the concentrations of the protein sample and the injected peptide. If the estimated protein and peptide concentrations differ from the true values by factors of α and β, then the fitted values of N_b, ΔH_D, and K_D differ from the true values by factors of $\alpha^{-1}\beta$, β^{-1}, and β, respectively.[64] Therefore, the fitted values of ΔH_D and K_D are not affected by errors in the estimated protein concentration, but are quite sensitive to errors in the estimated concentration of injected peptide. Errors in peptide (but not protein) concentration result in systematic deviations between temperature-dependent ΔH_D, ΔS_D, and K_D values and curves generated using any set of ΔH_0, ΔS_0, and ΔC_p. These systematic deviations can be corrected by allowing the peptide concentration to vary as an adjustable parameter in the temperature-dependent ΔC_p fits. Because all ITC experiments were performed with the same stock of dissolved peptide, it was only necessary to fit a single peptide concentration correction factor, β, for all temperatures.

The values of ΔH_0, ΔS_0, ΔC_p, and β were extracted by minimizing the chi-squared function

$$\chi^2 = \sum_T \frac{(\Delta H_D^{calc}(T) - \Delta H_D^{exp}(T))^2}{\sigma_H^2(T)} + \sum_T \frac{(\Delta S_D^{calc}(T) - \Delta S_D^{exp}(T))^2}{\sigma_S^2(T)} + \sum_T \frac{(K_D^{calc}(T) - K_D^{exp}(T))^2}{\sigma_K^2(T)} \quad (25)$$

where,

$$\Delta H_D^{calc}(T) = \beta^{-1}(\Delta H_0 + \Delta C_p(T - T_0)) \quad (26)$$

$$K_D^{calc}(T) = \beta \exp\left\{\frac{-1}{RT}\left(\Delta H_0 + \Delta C_p(T - T_0) - T\left(\Delta S_0 + \Delta C_p \ln \frac{T}{T_0}\right\}\right)\right) \quad (27)$$

and

$$\Delta S_D^{calc}(T) = \frac{\Delta H_D^{calc}(T)}{T} + R \ln K_D^{calc}(T) \quad (28)$$

Errors in ΔH_0, ΔS_0, ΔC_p, and β were estimated by Monte Carlo simulations with 12 136 iterations, where the uncertainty in each ΔH_D, ΔS_D, and K_D point was obtained from eq 24. The extracted value of $\beta = 0.85 \pm 0.02$ indicates that the peptide concentration determined by amino acid analysis underestimated the true concentration by approximately 15%. Under ideal conditions, the uncertainty in amino acid analysis is less than 5%.[47] However, in practice, errors in amino acid analyses performed at core laboratories are typically 10% to 15%,[46] which agrees well with the value of β we obtain. The χ^2 obtained with $\beta = 1$, i.e., no peptide concentration adjustment, is about 6.7-fold greater than that with $\beta = 0.85$. Note that experimental, i.e., uncorrected, thermodynamic parameters are listed in Table 1 and plotted in Figure 5. The true values of ΔH_D and K_D are related to the experimental values by factors of β and β^{-1}, respectively. A corrected value of the equilibrium dissociation constant, K_D^{corr}, was used to calculate the association rate constant according to the following:

$$k_{on} = \frac{k_{off}}{K_D^{corr}} = \frac{k_{off}}{\beta^{-1}K_D} \quad (29)$$

where K_D is the experimental equilibrium dissociation constant.

Monte Carlo Error Analysis. Monte Carlo (MC) error analyses were performed by repeating minimization calculations on MC data sets generated according to the following:

$$X_j^{MC} = X_j^{exp} + \sigma_j \varepsilon \quad (30)$$

where X_j is the jth experimental datum with experimental uncertainty σ_j and ϵ is drawn randomly from a normal distribution with a mean of zero and standard deviation of one. Errors in $\Delta H_A^{\ddagger}$, $\Delta H^{\ddagger}_D$, r_h, and ZZ-exchange-derived kinetic parameters were obtained with this method. In the case of ITC data, uncertainties in K_A and ΔH_D are correlated according to the covariance matrix, $\hat{V}_{post}$. This was taken in to account by generating MC data sets according to the following:[66]

$$\begin{bmatrix} \Delta H_D^{MC} \\ K_A^{MC} \end{bmatrix} = \begin{bmatrix} \Delta H_D^{exp} \\ K_A^{exp} \end{bmatrix} + \hat{L}\begin{bmatrix} \varepsilon \\ \delta \end{bmatrix} \quad (31)$$

where ϵ and δ are drawn randomly from normal distributions with means of zero and standard deviations of one, $\hat{L}$ is the lower-triangular matrix determined by Cholesky decomposition satisfying:

$$\hat{V}_{post} = \hat{L}\hat{L}^T \quad (32)$$

and $\hat{L}^T$ is the transpose of $\hat{L}$. Errors in β, ΔH_0, ΔS_0, and ΔC_p were calculated by applying eqs 20−28 to K_A^{MC} and ΔH_D^{MC} MC data sets.

Results and Discussion

Temperature Dependence of NMR Spectra. We employed a single NMR sample of ^{15}N-enriched Fyn SH3 domain that was partially saturated with a target peptide (VSLARRPLPPLP)[36] for the binding kinetic experiments. As discussed elsewhere, the molar ratio of protein to ligand affects the overall kinetics of exchange, due to the concentration dependence of the pseudo first-order association rate, k_{on}[X].[67] It was difficult to directly monitor the protein:peptide ratio, since the peptide lacks a fluorophore. Amino acid analysis was used to estimate the initial concentrations of peptide stock solutions; however, some loss of material is expected during subsequent handling steps. Therefore, in the fits below, the population of the bound state was allowed to vary as an adjustable parameter. Values determined by ZZ-exchange and CPMG methods were reasonably similar, 55% and 74%, respectively, therefore we conclude that the ratio of protein:peptide concentrations in the sample was close to 3:2. At low temperatures (10 and 20 °C), exchange was slow enough for separate bound and free protein peaks to be observed in ^{1}H−^{15}N correlation spectra. At higher temper-

(66) Amsler, C.; et al. *Phys. Lett. B* **2008**, *667*, 1–8.

Table 1. Summary of Thermodynamic and Kinetic Parameters for the Fyn SH3 Domain/Peptide Interaction

T (°C)	K_D (nM)[a]	ΔH_D (kcal mol^{-1})[b]	ΔS_D (cal mol^{-1} K^{-1})[c]	k_{off} (s^{-1})[d]	k_{on} ($\times$ 10^8 M^{-1} s^{-1})[e]	$D_{protein}$ ($\times$ 10^{-6} cm^2 s^{-1})[f]	$D_{peptide}$ ($\times$ 10^{-6} cm^2 s^{-1})[g]
10	37.5 ± 0.2	11.2 ± 0.4	5 ± 1	4.5 ± 0.2	1.03 ± 0.05	1.55 ± 0.03	0.78 ± 0.03
20	81 ± 16	13.8 ± 0.7	14 ± 3	11.7 ± 0.8	1.2 ± 0.3	2.1 ± 0.1	1.08 ± 0.02
30	161 ± 8	19.6 ± 0.7	34 ± 2	27.5 ± 0.6	1.44 ± 0.08	2.84 ± 0.05	1.46 ± 0.03
35	272 ± 19	21.8 ± 0.5	41 ± 2	62 ± 2	1.9 ± 0.1		
40	442 ± 28	23 ± 1	44 ± 4	117 ± 3	2.2 ± 0.2		
45				175 ± 2			
50	1388 ± 196	27 ± 1	56 ± 4	331 ± 5	2.0 ± 0.3		

[a] Equilibrium dissociation constant determined by ITC. [b] Molar enthalpy change upon dissociation determined by ITC. [c] Molar entropy change upon dissociation determined by ITC. [d] Dissociation rate constant determined by NMR. Value at 20 °C is the error-weighted average of CPMG- and ZZ-exchange-derived values. [e] Association rate constant determined by NMR and ITC according to eq 29. [f] Translational diffusion constant of the Fyn SH3 domain determined by NMR. [g] Translational diffusion constant of the 12 residue peptide determined by NMR.

atures, the kinetics of exchange were more rapid. Amide resonances with large chemical shift differences (>100 Hz) between the bound and free states were broadened beyond detection, while resonances with smaller chemical shift differences coalesced into single peaks.

ZZ Magnetization Exchange Experiments. At 10 and 20 °C, separate peaks for the free and bound forms of the Fyn SH3 domain could be observed and ZZ-magnetization exchange experiments were used to measure the kinetics of binding.[40] These are essentially inverse-detection ^{1}H−^{15}N correlation experiments, with an adjustable delay of duration T_{mix} inserted between the ^{15}N chemical shift encoding period and the direct acquisition of the ^{1}H signal, during which the signal of interest is stored as longitudinal ^{15}N magnetization. Any free protein that binds peptide during T_{mix} gives rise to a cross-peak at the ^{15}N chemical shift of the free form and the ^{1}H chemical shift of the bound form, and vice-versa. Each amide group in the protein can therefore produce four peaks in this experiment: two autopeaks corresponding to the free and bound forms, and two cross-peaks that are produced by peptide binding and release. The intensities of autopeaks and cross-peaks vary as a function of the mixing time T_{mix} and depend on the dissociation rate, k_{off}, the fractional population of the bound state, p_B,

$$p_B = \frac{k_{on}[X]}{k_{off} + k_{on}[X]} \tag{33}$$

and the ^{15}N longitudinal relaxation rates. We restricted our analysis to residues for which both auto- and both cross-peaks are clearly resolved, which comprised seven residues at 10 °C and twelve residues at 20 °C.

In order to extract dynamical parameters, ZZ exchange data are usually fit to analytical equations that neglect exchange during magnetization transfer steps.[19,40] This is a reasonable assumption for slowly exchanging systems, however in this case, the binding kinetics are rapid such that significant exchange occurs during the magnetization transfer steps. This is particularly evident in the appearance of cross-peaks with the delay period, T_{mix}, set to zero. Therefore, we fit the data numerically as described in the Experimental Section, extracting values of p_B and k_{off} for each residue on an individual basis. The data for all residues were then fit together, using global values of p_B and k_{off}. The group fitting increased the residual sum of squares by factors of only 1.08 (10 °C) and 1.20 (20 °C), compared to the individual fits, and excellent agreement between the experimental and back-calculated intensities was obtained, as shown in Figure 1. Dissociation rate constants extracted from the group fits are listed in Table 1.

CPMG Experiments. Backbone ^{15}N CPMG relaxation dispersion experiments[55] were used to quantify the kinetics of Fyn SH3 domain binding at 20, 30, 35, 40, 45, and 50 °C. These experiments suppress the contributions of millisecond time scale chemical shift fluctuations to ^{15}N transverse relaxation rates, R_2, using trains of 180° refocusing pulses.[19] Assuming that the chemical shift fluctuations are due to association and dissociation events following eq 1, R_2 will vary according to the delay between refocusing pulses (τ_{cp}) in a manner that depends on p_B, k_{off}, and the difference in precession frequency between the free and bound states, $\Delta\omega$. Analytical expressions have been derived for fitting relaxation dispersion profiles of R_2 versus $\nu_{CPMG} = 1/(2\tau_{cp})$ in various kinetic regimes.[68−70] The time scale of exchange is typically described using the parameter k_{ex},

$$k_{ex} = (k_{off} + k_{on}[X]) = \frac{k_{off}}{1 - p_B} \tag{34}$$

Under intermediate exchange conditions, where $k_{ex} \leq \Delta\omega$, values of k_{off}, p_B, and $\Delta\omega$ may be extracted directly from the fits of relaxation dispersion profiles. Under fast exchange conditions, where $k_{ex} > \Delta\omega$, the values of p_B and $\Delta\omega$ become codependent and cannot be extracted separately from the fits.[19] Instead, the parameters k_{ex} and Φ_{ex} are obtained, where,

$$\Phi_{ex} = p_B(1 - p_B)\Delta\omega^2 \tag{35}$$

We fit the CPMG data by solving modified Bloch−McConnell equations numerically as described in the Experimental Section, using three models of increasing restriction.

For Model 1, each residue was fit independently at each temperature, yielding residue-specific values of p_B, k_{off}, and $\Delta\omega$ in the case of intermediate exchange, and residue-specific values of k_{ex} and Φ_{ex} in the case of fast exchange. This model does not correspond to a global two-state binding process since exchange at each residue is treated independently. The estimates of the exchange parameters obtained using Model 1 are of low precision, since the fits are highly unrestrained. We used the residual chi-squared values obtained from Model 1 as a benchmark for the goodness of fit provided by subsequent models and did not further interpret the other parameters.

For Model 2, data at each temperature were analyzed assuming a global two-state process, which increases the

(67) Sugase, K.; Lansing, J. C.; Dyson, H. J.; Wright, P. E. *J. Am. Chem. Soc.* **2007**, *129*, 13406–13407.
(68) Luz, Z.; Meiboom, S. *J. Chem. Phys.* **1963**, *39*, 366.
(69) Carver, J. P.; Richards, R. E. *J. Magn. Reson.* **1972**, *6*, 89–105.
(70) Tollinger, M.; Skrynnikov, N. R.; Mulder, F. A.; Forman-Kay, J. D.; Kay, L. E. *J. Am. Chem. Soc.* **2001**, *123*, 11341–11352.

precision of the extracted parameters. For example, the uncertainties in global values of k_{ex} obtained with Model 2 are reduced by factors of 5 to 10 compared to those of Model 1. Such collective models have been successfully used to analyze CPMG data for a variety of different systems.[20,60,71] At 20 and 30 °C, exchange was in the intermediate regime for all residues; global values of p_B and k_{off} were extracted from the fits at each temperature, and $\Delta\omega$ values were obtained on a per-residue basis. At 35, 40, 45, and 50 °C, exchange shifted toward the fast regime due to the increase of the dissociation rate with increasing temperature. The exchange rate, k_{ex}, was fit globally at each temperature, and values of Φ_{ex} were obtained on a per-residue basis. As discussed below, the good agreement of the extracted Φ_{ex} and $\Delta\omega$ values with HSQC-derived chemical shifts, as well as the similar magnitudes of residual chi-squared parameters obtained with Models 1 and 2 suggest that a mechanism of concerted two-state exchange between the free and bound states is sufficient to account for the CPMG data.

For Model 3, additional constraints were imposed on the exchange equations in order to fit dissociation rate constants, k_{off}, with the highest possible level of precision. The values of $\Delta\omega$ were held fixed according to the differences in ^{15}N chemical shift between the free and peptide-saturated protein HSQC spectra. In addition, the population of the bound state, p_B, was constrained to be equal at all temperatures. This assumption is justified since the same sample was used in all cases, and the concentration of free protein, [P], was more than 100-fold greater than the equilibrium dissociation constant, K_D. Under these conditions, almost all of the peptide is bound, $[PX] \approx [X]_{total}$, and p_B is determined solely by the peptide:protein molar ratio, which is temperature-independent,

$$p_B = \frac{[PX]}{[P]_{total}} \approx \frac{[X]_{total}}{[P]_{total}} \tag{36}$$

Since the molar ratio is difficult to determine precisely by external measurements, we optimized this parameter using CPMG data and arrived at 0.74, as described in the Experimental Section. The residual χ^2 values obtained with Model 3 are about twice as large as those obtained from Models 1 and 2. This increase is not due to the constrained value of p_B, since allowing it to vary independently for each temperature while keeping the values of $\Delta\omega$ fixed does not significantly reduce the residual χ^2. The difference in χ^2 between Models 2 and 3 is therefore due to the fixed values of $\Delta\omega$. This is not surprising, since the agreement of CPMG- and HSQC-derived chemical shift differences is close, but not exact, due to uncertainties in both data sets. These discrepancies produce contributions to the residual χ^2 of Model 3 that are not present in those of Models 1 and 2. However, fixing $\Delta\omega$ values provides an advantage that outweighs this increase in χ^2. It resolves the codependence of $\Delta\omega$ and p_B values for residues in the fast exchange regime, so that these data can be included in the global p_B optimization, and it allows k_{off} to be extracted directly from fits involving these residues. Despite the increase in χ^2, the agreement between experimental CPMG data and those back-calculated using Model 3 remains excellent, as shown in Figure 2. In addition, the value of k_{off} obtained at 20 °C using Model 3 (11.2 ± 0.4 s^{-1}) closely matches the ZZ-exchange-derived value (12.8 ± 0.5 s^{-1}).

Two-State versus Multi-State Kinetics. We tested the applicability of a two-state exchange model to the binding reaction in a number of different ways. First, we investigated the presence of pre-existing conformational equilibria in the SH3 domain by performing CPMG experiments on the free protein at 30 and 50 °C. These measurements produced flat dispersion profiles for all residues, implying that ^{15}N chemical shifts do not experience significant fluctuations on the millisecond time scale in the absence of peptide. Therefore, any alternative conformations of the free protein are either present at low populations (<0.5%), exchange extremely rapidly (>10^4 s^{-1}), or have identical ^{15}N chemical shifts to the major conformer. We repeated these experiments at the same temperatures for a protein sample saturated with peptide at a 1:1.5 protein:peptide molar ratio, to test for the existence of partly bound states in exchange with the fully bound complex. The dispersion profiles were flat in this case as well, implying that millisecond time scale fluctuations of ^{15}N chemical shifts are absent in the complex. Thus, any partly bound states are either present at low populations (<0.5%), exchange with the bound complex extremely rapidly (>10^4 s^{-1}), or have identical ^{15}N chemical shifts to the bound complex. A further piece of evidence that binding is effectively two-state is obtained from an inspection of the 2-dimensional ^{1}H−^{15}N NMR correlation spectra themselves. In all CPMG and ZZ-exchange spectra, as well as in a peptide titration performed at 30 °C, the only observable signals correspond to the free, bound, and exchange peaks at low temperatures, or coalesced peaks at high temperatures. We did not detect any additional peaks corresponding to binding intermediates, as has been observed for the interaction of an SH2 domain with phosphotyrosine-containing peptides.[28,29]

ZZ-exchange and CPMG data at all temperatures are consistent with a two-state binding model. The agreement of experimental peak intensities (Figure 1) and transverse relaxation rates R_2 (Figure 2) with those back-calculated using global two-state exchange models is excellent. For ZZ-exchange data, the total residual sum of squares obtained using global exchange parameters is only 1.14-fold greater than that obtained with per-residue exchange parameters. For CPMG data, residual χ^2 values obtained using the global exchange parameters of Model 2 are only 1.10-fold greater than those obtained with the per-residue exchange parameters of Model 1. In contrast, there are several examples of more complex systems that exchange among three or more states and produce NMR CPMG data that do not agree well with global two-state models.[20,30,60] A final test of whether the NMR data are consistent with a two-state binding is whether the chemical shift-dependent parameters, $\Delta\omega$ and Φ_{ex}, extracted from the CPMG fits using Model 2, agree with the absolute differences in ^{15}N chemical shift extracted from HSQC spectra of the free and peptide-saturated protein, $|\Delta\delta_{HSQC}|$. If the peak broadening observed in the partially bound sample is due entirely to exchange between the free and bound states, then a plot of CPMG- versus HSQC-derived chemical shift differences should be linear with a slope of 1. Such a plot is shown in Figure 3a for CPMG data obtained at 20 and 30 °C, and exhibits the good agreement expected for a two-state binding reaction. At 35, 40, 45, and 50 °C, the kinetics of the system enter the fast exchange regime, precluding the direct extraction of $\Delta\omega$ values. As discussed above, CPMG fits using Model 2 at these temperatures instead yield $\Phi_{ex} = p_B(1 - p_B)\Delta\omega^2$. Again, if peak broadening is due to two-state exchange between free and bound states, then a plot of $\sqrt{\Phi_{ex}}$ versus $\Delta\delta_{HSQC}$ should be linear with a slope of $(p_B\ (1 - p_B))^{1/2}$, as is observed in Figure 3b. Notably, plots of the data obtained at temperatures from 35 to 50 °C coincide and are therefore consistent with the same value of p_B. Taken together, these observations indicate that binding of the Fyn SH3

(71) Mulder, F. A. A.; Mittermaier, A.; Hon, B.; Dahlquist, F. W.; Kay, L. E. *Nat. Struct. Biol.* **2001**, *8*, 932–935.

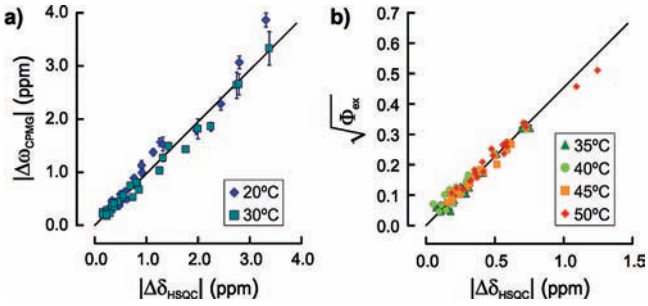

Figure 3. Chemical shift differences, $\Delta\omega_{CPMG}$, extracted from fits of ^{15}N CPMG data at 20 and 30 °C plotted as a function of the absolute difference in ^{15}N chemical shift, $|\Delta\delta_{HSQC}|$, between the free and ligand-saturated forms of the Fyn SH3 domain **(a)**. The line in (a) passes through the origin with a slope of 1. Plot of $\sqrt{\Phi_{ex}} = (p_B\,(1 - p_B))^{1/2}\,\Delta\omega$ values extracted from fits of ^{15}N CPMG data at 35, 40, 45, and 50 °C versus absolute chemical shift differences, $|\Delta\delta_{HSQC}|$ **(b)**. The line in (b) passes through the origin with a least-squares optimized slope.

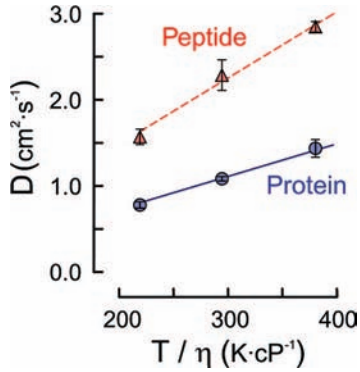

Figure 4. Translational diffusion constants, *D*, for the Fyn SH3 domain (circles) and VSLARRPLPPLP peptide (triangles) determined by NMR plotted as a function of temperature/viscosity.

domain to the peptide used in this study is effectively two-state in the sense that any binding intermediates are either weakly populated or in very rapid exchange with the free or bound states.

PFG Translational Diffusion Measurements. The translational diffusion coefficients of the protein and peptide were determined using 1D ^1H linear-encode-decode pulsed-field-gradient (LED-PFG) NMR experiments[62] at 10, 20, and 30 °C. In this method, transverse magnetization is encoded with a spatially dependent phase by a pulsed-field gradient. The signal is stored as longitudinal magnetization for a constant diffusion delay, and the phase is then decoded in a spatially dependent manner by a second pulsed-field gradient. Large gradient strengths, diffusion constants, and relaxation delays lead to large attenuation of the signal. The value of the diffusion constant can be extracted from the dependence of peak intensities on the strength of the gradients. We have plotted the translational diffusion constants thus obtained for protein and peptide as a function of T/η in Figure 4, where η is the solvent viscosity. If the molecules obey the Stokes−Einstein diffusion equation,

$$D = \frac{k_B T}{6\pi r_H \eta} \tag{37}$$

the graph is linear with a slope equal to $k_B/(6\pi r_H)$, where k_B is Boltzmann's constant and r_H is the hydrodynamic radius. Data for both protein and peptide closely follow straight lines with correlation coefficients of greater than 0.99. The corresponding values of the hydrodynamic radii of the protein, $r_H = 17.4 \pm 0.4$Å, and peptide, $r_H = 9.2 \pm 0.1$Å agree well with the expected values for a 75-residue globular protein and a 12-residue unstructured peptide.[72] These results indicate that both protein and peptide are monodisperse in solution. Significant levels of self-association would result in translational diffusion rates that are lower than those predicted for the monomeric components.[62] The good agreement of experimental diffusion rates with the Stokes−Einstein eq 37 also suggests that the frequency of random collisions between the protein and peptide should approach the Smoluchowski limit,[6,73] and be proportional to T/η, as discussed below.

Isothermal Titration Calorimetry. The thermodynamics of peptide binding to the Fyn SH3 domain were characterized by ITC at 10, 20, 30, 35, 40, and 50 °C. Multiple injections of a peptide solution were made into a sample of the Fyn SH3 domain, and an exothermic binding reaction was observed at all temperatures, as illustrated in Figure 5a. Good agreement was obtained by fitting the experimental isotherms to a simple two-state binding model, yielding the equilibrium dissociation constant, K_D, the enthalpy, ΔH_D, and entropy, ΔS_D, of dissociation at each temperature, as shown in Figure 5b. The temperature dependences of these parameters are governed by the difference in heat capacity between the free and bound states, ΔC_p, according to the following:

$$\Delta H_D = \Delta H_0 + \Delta C_p (T - T_0) \tag{38}$$

$$\Delta S_D = \Delta S_0 + \Delta C_p \ln\left\{\frac{T}{T_0}\right\} \tag{39}$$

and

$$K_D = \exp\left\{\frac{-\Delta H_D + T\Delta S_D}{RT}\right\} \tag{40}$$

where R is the molar gas constant, and ΔH_0 and ΔS_0 are the enthalpy and entropy of dissociation at a reference temperature, T_0. Plots of ΔH_D versus T and ΔS_D versus $\ln\{T\}$ are both linear with slopes of ΔC_p, while a van't Hoff plot of $\ln\{K_D\}$ versus T^{-1} has curvature determined by ΔC_p. The data set of ΔH_D, ΔS_D, and K_D values measured at 6 temperatures can be fit simultaneously to extract ΔH_0, ΔS_0, and ΔC_p. We found that in order to obtain good agreement between experimental and back-calculated thermodynamic parameters, it was necessary to also allow the concentration of injected peptide to vary as an adjustable parameter in the fits, as described in the Experimental Section. Since the same peptide stock solution was used for all ITC measurements, this introduced only a single additional parameter to fits of the complete ITC data set. With a 15% adjustment in the peptide concentration, excellent agreement was obtained between the ITC data at all temperatures and back-calculated values, as shown in Figure 5 c−e. Taking the 30 °C as the reference temperature, we found $\Delta H_0 = 15.4 \pm 0.3$ kcal mol^{-1}, $\Delta S_0 = 20 \pm 1$ cal mol^{-1} K^{-1}, and $\Delta C_p = 352 \pm 9$ cal mol^{-1} K^{-1}. These values are quite similar to those found in ITC studies of the Sem-5,[74] Abl,[75] and α-spectrin[76] SH3 domains. The large positive value of ΔC_p is consistent with the hydrophobic nature of the binding interface, which includes the peptide residues Pro7, Leu8, Pro9, Pro10, Leu11, and Pro12 adjacent to a hydrophobic patch on the SH3 domain surface composed of Tyr8, Tyr10, Trp36, Pro51, and Tyr54. Positive

(72) Wilkins, D. K.; Grimshaw, S. B.; Receveur, V.; Dobson, C. M.; Jones, J. A.; Smith, L. J. *Biochemistry* **1999**, *38*, 16424–16431.
(73) Smoluchowski, M. *Z. Phys. Chem.* **1917**, *92*, 129–168.
(74) Ferreon, J. C.; Hilser, V. J. *Biochemistry* **2004**, *43*, 7787–7797.
(75) Palencia, A.; Cobos, E. S.; Mateo, P. L; Martinez, J. C.; Luque, I. *J. Mol. Biol.* **2004**, *336*, 527–537.
(76) Casares, S.; AB, E.; Eshuis, H.; Lopez-Mayorga, O.; van Nuland, N. A. J.; Conejero-Lara, F. *BMC Struct. Biol* **2007**, *7*, 22–40.

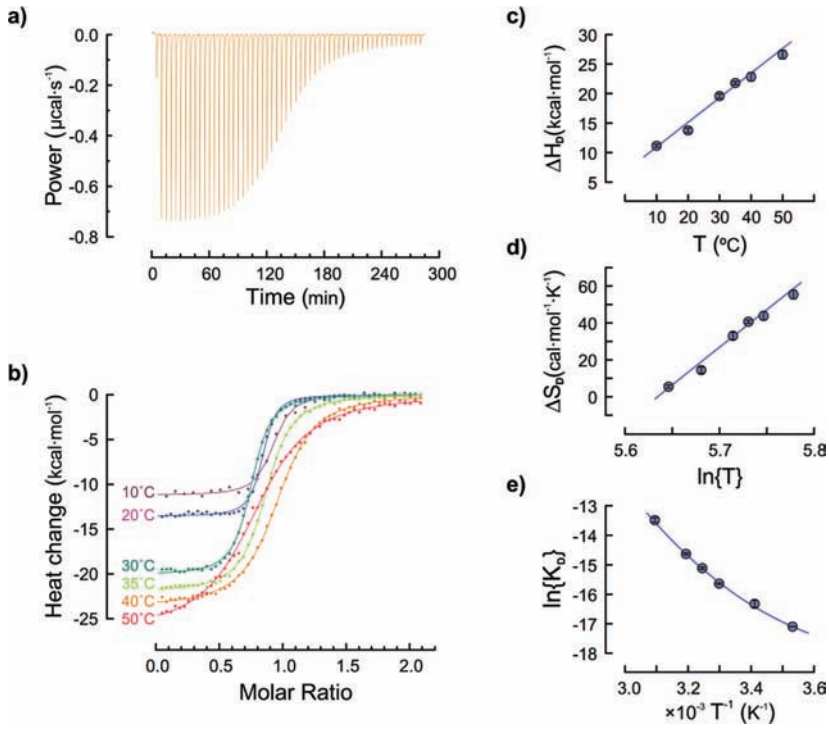

Figure 5. Baseline-subtracted raw ITC data for injections of VSLARRPLPPLP peptide into a solution of the Fyn SH3 domain at 40 °C (**a**). Fits of ITC data to a simple two-state binding model **(b)**. Enthalpies of dissociation plotted as a function of reaction temperature **(c)**. Entropies of dissociation plotted as a function of ln{T} **(d)**. van't Hoff plot of equilibrium dissociation constants **(e)**. Lines and curve in (c)−(e) were generated with eqs 26−28 using optimized values of ΔH_0, ΔS_0, ΔC_p, and β.

values of ΔC_p in protein folding and binding are usually associated with the solvation of nonpolar groups.[77] Dissociation of the peptide likely results in an increase in the solvent exposure of hydrophobic residues of both the protein and peptide and a concomitant increase in heat capacity.

Association and Dissociation Rate Constants. Protein association can be described using the following kinetic scheme[6,78−82]

$$P + X \underset{k_{-1}}{\overset{k_1}{\rightleftharpoons}} P:X + X \underset{k_2}{\overset{k_2}{\rightleftharpoons}} PX \qquad (41)$$

where PX refers to the bound state and P:X refers to the transient encounter complex, which may be thought of as an ensemble of molecular arrangements present at the end-point of translational diffusion.[83] The free energy of the encounter complex is large compared to that of the bound state, so that binding according to this model can still be considered two-state, with only the bound and/or free states having significant populations. The second-order rate constant k_1 describes the frequency with which the two binding surfaces are brought into favorable contact through random collisions, resulting in formation of an encounter complex. Dissociation of the encounter complex occurs with a rate constant k_{-1}, while rearrangement of the encounter complex into the bound state occurs with a rate constant k_2. Under steady-state conditions, the association and dissociation rates are given by the following:

$$k_{on} = \frac{k_1 k_2}{k_{-1} + k_2} \qquad (42)$$

$$k_{off} = \frac{k_{-2} k_{-1}}{k_{-1} + k_2} \qquad (43)$$

In the diffusion limit, where the rearrangement step is much faster than the dissociation of the encounter complex, $k_2 \gg k_{-1}$, the macroscopic dissociation rate is determined by the stability and dissociation rate of the encounter complex, $k_{off} = k_{-2}/k_2$ k_{-1}, while the association rate depends simply on the frequency of productive collisions, $k_{on} = k_1$. Values of k_1 can vary from over 10^9 M^{-1} s^{-1}, for electrostatically assisted binding reactions[78] to a lower limit of about 10^5 M^{-1} s^{-1}, which is largely determined by the geometric specificity of the encounter complex.[84−86] The productive collision frequency, k_1, is proportional to the sum of the translational diffusion constants of the protein and ligand.[6] Therefore, in the diffusion limit, the temperature dependence of k_{on} is governed by T/η, according to eq 37, and the activation enthalpy of association is close to the characteristic value for a diffusion-limited reaction in water, approximately 4.5 kcal mol^{-1}.[87] Although electrostatic enhancement of binding could potentially influence the temperature dependence of k_{on}, this effect does not appear to be large, since diffusion-limited protein association rates show apparent activa-

(77) Prabhu, N.; Sharp, K. *Annu. Rev. Phys. Chem.* **2005**, *56*, 521–548.
(78) Alsallaq, R.; Zhou, H. X. *Prot. Struct. Funct. Bioinf.* **2008**, *71*, 320–335.
(79) Selzer, T.; Schreiber, G. *J. Mol. Biol.* **1999**, *287*, 409–419.
(80) Vijayakumar, M.; Wong, K. Y.; Schreiber, G.; Fersht, A. R.; Szabo, A.; Zhou, H. X. *J. Mol. Biol.* **1998**, *278*, 1015–1024.
(81) Berg, O. G *Biophys. J.* **1985**, *47*, 1–14.
(82) Solc, K.; Stockmayer, W *Int. J. Chem. Kinet.* **1973**, *5*, 733–752.
(83) Gabdoulline, R. R.; Wade, R. C. *J. Mol. Recognit.* **1999**, *12*, 226–234.
(84) Northrup, S. H.; Erickson, H. P. *Proc. Natl. Acad. Sci. U.S.A.* **1992**, *89*, 3338–3342.
(85) Zhou, H. X *Biophys. J.* **1997**, *73*, 2441–2445.
(86) Schlosshauer, M.; Baker, D. *Protein Sci.* **2004**, *13*, 1660–1669.
(87) Pilling, M.; Seakins, P. *Reaction Kinetics*; Oxford University Press: Oxford, 1995.

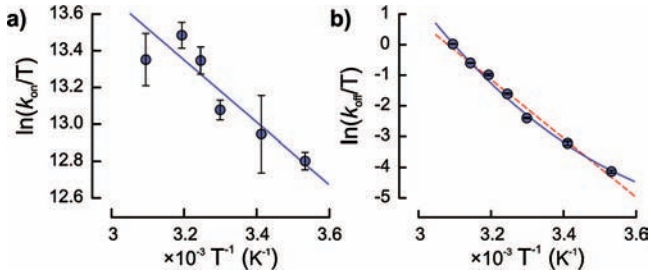

Figure 6. Eyring plot of association rate constants calculated from ITC and NMR data according to eq 2 (**a**). Eyring plot of NMR-derived dissociation rate constants (**b**). The solid curve and dashed line correspond to fits of the data with $\Delta C_p^{\ddagger} = 352$ cal mol^{-1} K^{-1} and $\Delta C_p^{\ddagger} = 0$, respectively, as described in the text.

tion enthalpies of 4 to 10 kcal mol^{-1}, in agreement with the Stokes−Einstein relationship,[88−90] even when electrostatics are known to play a large role, as for barnase and barstar.[8] Thus, diffusion-limited binding reactions are characterized by association rate constants greater than 10^5 M^{-1} s^{-1}, and apparent activation enthalpies of about 4.5 kcal mol^{-1}.[91]

Second-order association rate constants, k_{on}, were calculated from the NMR-derived dissociation rate constants, k_{off}, and corrected equilibrium dissociation constants, K_D, following eq 29. Values of k_{on} do not vary significantly with temperature, and range from 1.03 $\times$ 10^8 M^{-1} s^{-1} at 10 °C to 2.0 $\times$ 10^8 M^{-1} s^{-1} at 50 °C, implying that association does not involve a large enthalpic barrier. The association rates are similar to those of other protein−ligand complexes whose association is believed to be diffusion-limited.[4] An Eyring plot of $\ln\{k_{on}/T\}$ versus T^{-1}, shown in Figure 6a, has a slope of $-\Delta H_A^{\ddagger}/R$, where $\Delta H_A^{\ddagger}$ is the activation enthalpy of association. The level of agreement between the experimental points and the linear fit is quite encouraging, considering that the values of k_{on} vary by only a factor of 2 over the entire temperature range, and that they are obtained from a combination of ZZ-exchange and CPMG NMR kinetic experiments and ITC equilibrium measurements. The activation enthalpy of association, $\Delta H_A^{\ddagger} = 3.4 \pm 0.5$ kcal mol^{-1}, obtained from the slope of the plot is close to the expected value for a diffusion-limited binding reaction. This suggests that peptide binding by the Fyn SH3 domain is in the diffusion-limited regime, i.e., that the folding and docking of the peptide and the rearrangement of the binding site occur rapidly compared to the dissociation of the encounter complex.

NMR-derived first-order dissociation rate constants, k_{off}, show a strong temperature dependence, varying from 4.5 s^{-1} at 10 °C to 331 s^{-1} at 50 °C, implying that dissociation involves a significant enthalpic barrier. The kinetics in this system are much more rapid than those of other protein/ligand interactions for which the binding mechanism has been studied in detail. For example, the average survival time of the SH3 domain/peptide complex is just 3 ms at 50 °C. This is about 7 orders of magnitude shorter than that of the well-characterized complex between barnase and its inhibitor barstar, which survives 35 h on average before dissociation.[10] The Eyring plot of dissociation rates, shown in Figure 6b, exhibits similar curvature to that of the van′t Hoff plot in Figure 5e. A model to explain this curvature can be derived in terms of the reaction scheme given in eq 41. Assuming that $k_2 \gg k_{-1}$ and that k_{-1} follows Eyring kinetics,[92] the dissociation rate is given by the following:

$$k_{off} = \frac{k_B T}{h} \exp\left\{\frac{-\Delta G^{\ddagger}}{RT}\right\} \tag{44}$$

where $\Delta G^{\ddagger} = G^{TS} - G^{PX}$, G^{PX} is the free energy of the bound state, and G^{TS} is the free energy of the transition state separating the encounter complex (P:X) and the free state ($P + X$). Curvature of the k_{off} Eyring plot is consistent with a hydrophobic protein/peptide interface that is solvated at the rate-limiting step of dissociation, such that the heat capacity of the transition state, C_p^{TS}, is greater than that of the bound state C_p^{PX}. As mentioned previously, large changes in heat capacity are usually thought to accompany changes in molecular solvation.[77] We tested whether the curvature of the Eyring plot matches the ITC-derived value of ΔC_p (352 cal mol^{-1} K^{-1}) by fitting eqs 38, 39, and 44 to the experimental k_{off} values, replacing ΔH_D, ΔS_D, and ΔC_p with $\Delta H_D^{\ddagger} = H^{TS} - H^{PX}$, $\Delta S_D^{\ddagger} = S^{TS} - S^{PX}$, and $\Delta C_p^{\ddagger} = C_p^{TS} - C_p^{PX}$, and fixing $\Delta C_p^{\ddagger} = 352$ cal mol^{-1} K^{-1}. The curved fit with $\Delta C_p^{\ddagger} = 352$ cal mol^{-1} K^{-1} provides better agreement with the experimental data than a linear fit with $\Delta C_p^{\ddagger} = 0$, and the residual chi-squared is lower by a factor of about 2.6. This suggests that the hydrophobic portion of the protein/peptide interface is largely disrupted, and the nonpolar groups it contains are hydrated during the rate-determining step of dissociation. In other words, resolvation of the hydrophobic interface is a relatively early event in the dissociation process. Interestingly, this has also been observed for the dissociation pathway of barnase and barstar,[88] even though k_{off} values for this system are about 7 orders of magnitude smaller than the ones obtained here.

The results presented here largely agree with recent computer simulations of the binding reaction between the N-terminal SH3 domain from the Crk adaptor protein and a proline-rich peptide.[93] The calculations were initiated from the unbound state with at least 13 Å separation between the protein and peptide. Six out of thirteen simulations resulted in the formation of tight, stereospecific complexes. The strong tendency of the protein and peptide to proceed to the bound state even with large initial separations is consistent with our observation of a highly solvated transition state. In addition, these simulations found the peptide binding mechanism to consist of two distinct stages, analogous to eq 41. The first step involved the rapid formation of an electrostatically stabilized encounter complex, while the second step involved the docking of the peptide into the binding site and the formation of a stable bound structure. Once formed, the encounter complex did not dissociate in any of the simulations, while docking of the peptide occurred rapidly (<50 ns). This is consistent with our observation of a diffusion-limited reaction, with $k_2 \gg k_{-1}$ in eq 41.

Other groups have measured the kinetics of peptide binding by SH3 domains. Recently, Kay and co-workers used a suite of CPMG-based NMR experiments to characterize the interaction between the Abp1 SH3 domain and a fragment of the yeast Ark1p protein, obtaining a dissociation rate constant, k_{off}, of about 230 s^{-1} at 25 °C.[94] Combining this number with a dissociation constant of 0.55 μM,[95] the association rate constant, k_{on}, is 4.2 $\times$ 10^8 M^{-1} s^{-1}, which agrees well with our results. This contrasts with a number of SH3 domain studies performed using surface plasmon resonance (SPR), which have found much slower association and

(88) Frisch, C.; Fersht, A.; Schreiber, G. *J. Mol. Biol.* **2001**, *308*, 69–77.
(89) Raman, C.; Jemmerson, R.; Nall, B.; Allen, M. *Biochemistry* **1992**, *31*, 10370–10379.
(90) Xavier, K. A.; Willson, R. C *Biophys. J.* **1998**, *74*, 2036–2045.
(91) Gabdoulline, R. R.; Wade, R. C. *Methods* **1998**, *14*, 329–341.
(92) Castellan, G. *Physical Chemistry*, 3rd ed.; Benjamin Cummings: Menlo Park, CA, 1983.
(93) Ahmad, M.; Gu, W.; Helms, V. *Angew. Chem., Int. Ed.* **2008**, *47*, 7626–7630.
(94) Hansen, D. F.; Vallurupalli, P.; Lundstrom, P.; Neudecker, P.; Kay, L. E. *J. Am. Chem. Soc.* **2008**, *130*, 2667–2675.

dissociation rate constants, on the order of 10^3 to 10^5 M^{-1} s^{-1} and 10^{-2} to 10^{-3} s^{-1}, respectively.[96−100] Notably, a recent SPR study of the Fyn SH3 domain and type I ligands derived from Csk binding protein (Cbp/PAG) determined association rate constants of about 7×10^4 M^{-1} s^{-1}, which are more than 1000-fold slower than those observed here.[101] One explanation for this discrepancy is that the peptide/protein pairs chosen for SPR analysis simply happen to have much slower binding kinetics than the systems studied by NMR. Another possibility is that the systems studied by SPR do, in fact, follow similar kinetics to those observed by NMR, but that the SPR measurements are not reflective of solution-state association and dissociation rates. In SPR experiments, the mass transport of ligand into the hydrated matrix containing the immobilized binding partner, and impeded diffusion of the ligand within this phase, can dominate the binding kinetics when the intrinsic reaction rate is greater than 10^6 M^{-1} s^{-1}.[102] This is well below the NMR-derived k_{on} values for SH3 domains. In such cases, the kinetic parameters determined by SPR can underestimate the true values by several orders of magnitude.[103] This underlines one of the advantages of equilibrium, solution-state NMR binding measurements. They do not rely on the net transfer of molecules from one phase to another and therefore do not suffer from mass transport artifacts.

SH3 domains play important roles in a wide variety of cellular processes. Interactions between SH3 domains and proline-rich targets mediate the formation of protein complexes involved in cell signaling and actin filament organization, and help to localize SH3-containing proteins and their binding partners to specific subcellular compartments such as the cytoskeleton or membrane ruffles.[34,37] SH3 domains participate in mitogenesis,[31] T-cell activation,[104] and cell polarization[34] by bringing together partners in signaling cascades and by directly governing enzyme activity. For example, Fyn belongs to the Src family of tyrosine kinases, whose members contain an SH3 and SH2 domain separated from the catalytic domain by a linker region.[105] In the inactive form of these enzymes, the SH3 domain binds a target sequence in the linker region and the SH2 domain binds a phosphotyrosine-containing sequence at the C-terminus, which locks the kinase domain in a closed conformation.[106−109] The enzyme can be activated by displacement of the intramolecular target from the SH3 domain by a proline-rich region of another protein.[110,111]

The affinities of SH3 domain/peptide interactions are relatively weak, considering their importance to cellular control. K_D values for synthetic target peptides are generally in the low μM range.[37] It has been suggested that the low affinity of SH3 domain interactions could play a functional role, by maintaining high rates of dissociation and allowing protein−protein interactions to be rapidly remodeled in response to changing cellular conditions.[37,104] Notably, SH3 domain binding kinetics determined by SPR are well below the diffusion limit, and are therefore not consistent with this hypothesis. In contrast, our results obtained using NMR and ITC suggest that, in fact, SH3 domain interactions are optimized for the rapid assembly and disassembly of protein complexes. We find that association rates for the Fyn SH3 domain are close to the theoretical limit, and match those of cytotoxic nuclease/inhibitor complexes where rapid binding is thought to be critical for cell survival.[8,12] Fast association rates, in turn, allow maximal dissociation rates for a given affinity. Thus, the fast binding kinetics observed in this study are optimal for rapid responses of SH3-mediated interactions to changing intracellular signals.

Conclusions

We used NMR CPMG and ZZ-exchange experiments in conjunction with ITC to characterize the interaction between the Fyn SH3 domain and a 12-residue peptide ligand. ITC data collected at 6 temperatures ranging from 10 to 50 °C are remarkably self-consistent and can be completely accounted for by 4 parameters: the enthalpy and entropy of dissociation, the difference in heat capacity between the free and bound states, and a correction factor for the concentration of injected peptide. The free protein and peptide have a significantly higher heat capacity than the bound complex, consistent with an increase in the exposure of nonpolar groups to solvent upon dissociation. On the basis of a number of criteria, the NMR data are consistent with a two-state binding mechanism, allowing us to describe the reaction simply with an association, k_{on}, and dissociation, k_{off}, rate constant. The temperature dependence of NMR-derived k_{off} values indicates that there is a significant energy barrier to dissociation. Curvature in the k_{off} Eyring plot closely matches the ITC-derived value of ΔC_p, which suggests that the hydrophobic binding interface is highly solvated upon reaching the rate-limiting-step of dissociation. The magnitudes and temperature dependence of association rate constants, k_{on}, are consistent with a diffusion-limited process. Such rapid binding rates may influence the kinetics of Fyn tyrosine kinase activation. The complex studied here has survival times on the millisecond time scale, and would be too short-lived to characterize using standard, nonequilibrium mixing techniques. However, the combination of NMR and ITC methodologies has allowed us study the binding mechanism in detail. This approach promises to extend our understanding of protein recognition to faster timescales.

Acknowledgment. This work was supported by the National Science and Engineering Research Council and a Canadian Institutes of Health Research Training Grant. We thank Lewis Kay for helpful discussions.

JA808255D

(95) Vallurupalli, P.; Hansen, D. F.; Stollar, E.; Meirovitch, e.; Kay, L. E *Proc. Natl. Acad. Sci. U.S.A.* **2007**, *104*, 18473–18477.
(96) Bhaskar, K.; Yen, S. H.; Lee, G. *J. Biol. Chem.* **2005**, *280*, 35119–35125.
(97) Kim, H. I.; Jung, J.; Lee, E. S.; Kim, Y. C.; Lee, W.; Lee, S. T. *Biochem. Biophys. Res. Commun.* **2007**, *362*, 829–834.
(98) Shelton, H.; Harris, M *Virology J.* **2008**, *5*, 24.
(99) Solomaha, E.; Szeto, F. L.; Yousef, M. A.; Palfrey, C *J. Biol. Chem.* **2005**, *280*, 23147–23156.
(100) Vidal, M.; Goudreau, N.; Cornille, F.; Cussac, D.; Gincel, E.; Garbay, C *J. Mol. Biol.* **1999**, *290*, 717–730.
(101) Solheim, S. A.; Petsalaki, E.; Stokka, A. J.; Russell, R. B; Tasken, K.; Berge, T *FEBS J.* **2008**, *275*, 4863–4874.
(102) Schuck, P. *Biophys. J.* **1996**, *70*, 1230–1249.
(103) Schuck, P.; Minton, A. P. *Anal. Biochem.* **1996**, *240*, 262–272.
(104) Li, S. C *Biochem. J.* **2005**, *390*, 641–653.
(105) Parsons, S. J.; Parsons, J. T. *Oncogene* **2004**, *23*, 7906–7909.
(106) Sicheri, F.; Moarefi, I.; Kuriyan, J. *Nature* **1997**, *385*, 602–609.
(107) Xu, W; Lei, A. D., M; Eck, M. J.; Harrison, S. C. *Mol. Cell* **1999**, *3*, 629–638.
(108) Xu, W.; Harrison, S. C.; Eck, M. J. *Nature* **1997**, *385*, 595–602.
(109) Yamaguchi, H.; Hendrickson, W. A. *Nature* **1996**, *384*, 484–489.
(110) Moarefi, I.; LaFevre-Bernt, M.; Sicheri, F.; Huse, M.; Lee, C. H.; Kuriyan, J.; Miller, W. T. *Nature* **1997**, *385*, 650–653.
(111) Lerner, E. C.; Smithgall, T. E. *Nat. Struct. Biol.* **2002**, *9*, 365–369.